Reliability Engineering and System Safety 124 (2014) 56–67

Contents lists available at ScienceDirect

Reliability Engineering and System Safety

journal homepage: www.elsevier.com/locate/ress

Accounting for future redesign to balance performance and development costs

D. Villanueva [a,b,*], R.T. Haftka [a], B.V. Sankar [a]

[a] University of Florida, P.O. Box 116250, Gainesville, FL 32611, United States
[b] Ecole des Mines de Saint-Etienne, 158 cours Fauriel, 42023 Saint-Etienne cedex 2, France

ARTICLE INFO

Article history:
Received 23 December 2012
Received in revised form
24 November 2013
Accepted 28 November 2013
Available online 6 December 2013

Keywords:
Future test
Redesign
Two-stage stochastic optimization

ABSTRACT

Most components undergo tests after they are designed and are redesigned if necessary. Tests help designers find unsafe and overly conservative designs, and redesign can restore safety or increase performance. In general, the expected changes to the performance and reliability of the design after the test and redesign are not considered. In this paper, we explore how modeling a future test and redesign provides a company an opportunity to balance development costs versus performance by simultaneously designing the design and the post-test redesign rules during the initial design stage. Due to regulations and tradition, safety margin and safety factor based design is a common practice in industry as opposed to probabilistic design. In this paper, we show that it is possible to continue to use safety margin based design, and employ probability solely to select safety margins and redesign criteria. In this study, we find the optimum safety margins and redesign criterion for an integrated thermal protection system. These are optimized in order to find a minimum mass design with minimal redesign costs. We observed that the optimum safety margin and redesign criterion call for an initially conservative design and use the redesign process to trim excess weight rather than restore safety. This would fit well with regulatory constraints, since regulations usually impose minimum safety margins.

1. Introduction

Traditionally, aerospace structures have been designed deterministically, employing safety margins and safety factors to protect against failure. After the design stage, most components undergo tests, whose purpose is to validate the model and catch unacceptable designs and redesign them. After production, inspection and manufacturing are done to ensure safety throughout the life cycle. In contrast, probabilistic design considers uncertainties to calculate the reliability, which allows the trade-off of cost and performance.

In recent years, there has been a movement to quantify the effect of uncertainty reduction measures, such as tests, inspection, maintenance, and health monitoring, on the safety of a product over its life cycle. Much work has been completed in the areas of inspection and maintenance for structures under fatigue [1–4]. A study reported by Acar et al. [5] investigated the effects of future tests and redesign on the final distribution of failure stress and structural design with varying numbers of tests at the coupon, element, and certification levels. Golden et al. [6] proposed a method to determine the optimal number of experiments required to reduce the variance of uncertain variables. Sankararaman et al. [7] proposed an optimization algorithm of test resource allocation for multi-level and coupled systems. A method to simultaneously design a structural component and the corresponding proof test considering the probability of failure and the probability of failing the proof test was introduced by Venter and Scotti [8].

Most aerospace components are designed using a computational modeling technique, such as finite element analysis. We expect some error, often labeled as epistemic uncertainty (associated with lack of knowledge), in the modeled behavior. The true value of this error is unknown, and thus we consider this lack of knowledge to lead to an uncertain future. Tests are performed to reduce the error, thus narrowing the range of possible futures through the knowledge gained and the correction of unacceptable futures by redesign.

Previously, Villanueva et al. [9] proposed a method to simulate these possible futures including test and redesign, and studied the effect of a single future thermal test followed by redesign on the initial reliability estimates of an integrated thermal protection system (ITPS). An ITPS is a structure on a reusable launch vehicle that simultaneously provides protection from aerodynamic heating during reentry, while working as a load bearing structure. Monte Carlo sampling of the assumed computational and

* Corresponding author at: University of Florida, P.O. Box 116250, Gainesville, FL 32611, United States. Tel.: +1 3523926780.
E-mail addresses: dvillanu@gmail.com (D. Villanueva), haftka@ufl.edu (R.T. Haftka), sankar@ufl.edu (B.V. Sankar).
URL: http://dianevillanueva.com (D. Villanueva).

0951-8320/$ - see front matter © 2013 Elsevier Ltd. All rights reserved.
http://dx.doi.org/10.1016/j.ress.2013.11.013

Nomenclature

d	design variable
e_c	computational error
e_x	experimental error
$f(T)$	probability distribution of the temperature
m	mass per unit area, kg/m^2
p_f	probability of failure, %
r	random variable
S	safety margin
ΔT	change in temperature, K
T	temperature, K

Subscripts

calc	calculated
corr	corrected
ini	initial
L	lower bound
nom	nominal
meas	measured
re	redesign
test	test article
true	true
U	upper bound

experimental errors was used to sample future test alternatives, or the possible outcomes of the future test. Using the future alternatives, the methodology included two methods of calibration and redesign. It was observed that the deterministic approach to calibration and redesign, which acted to restore the original (designed) safety margin, led to a greatly reduced probability of failure after the test and redesign, a reduction that usually is not quantified. A probabilistic approach was also presented, which provided a way to more accurately estimate the probability of failure after the test, while trading off weight against performing additional tests. Matsumura et al. [10] extended the methodology to include additional failure modes of the ITPS.

In this paper we use the reliability estimates of [9] as a building block to show that modeling future redesign provides a company with the opportunity to trade off development costs (test and redesign) and performance (mass) by designing the initial design criteria and the redesign rules. As regulations and tradition drive companies to use traditional deterministic design with safety margins and safety factors, we limit ourselves to deterministic design and redesign processes. The probabilistic approach can be limited to select safety margins and redesign criteria. This is a two-stage stochastic optimization problem [11], a type of problem which has been studied extensively in the area of process planning under uncertainty [12,13]. Here, in the first stage, a decision is made about the initial design before the test (i.e., an initial optimum design is found) and then decisions are taken based on the updated information from the test result (i.e., to redesign or not) in the second stage.

This research fits into a class of studies that have identified measures that are used to engineer safe designs and sought out ways to find an optimal set of safety policies or practices. Möller and Hansson [14] provided a review of safety practices (e.g., safety factor, safety margin, reliability) in engineering and how they increase safety. Aktas et al. [15] used cost and safety optimization to optimize load factors and safety indices considering the initial cost of design and future failure costs based on probability of failure for bridge specifications. Beck et al. [16] presented a method to optimize partial safety factors of the design of a steel beam under epistemic uncertainties in a robust optimization formulation considering costs of failure. In the same vein, we seek to optimize the design and redesign rules considering the outcome of a future test.

The following section of the paper will provide a description of the test problem, the integrated thermal protection system. Though the methods in this paper are focused on this particular example, they can be translated to any example problem in which the uncertainties in the computational model and experiment are quantifiable and the ranges of acceptable safety margins and safety factors are given. In Section 3, the process of test and redesign is described in detail. Section 4 provides a detailed description of the uncertainties considered in this study, and Section 5 describes how these uncertainties are used to obtain a distribution of the probability of failure. In Section 6, the process of simulating the future test and redesign for a single candidate design is described. An illustrative example is provided in Section 7.

2. Integrated thermal protection shield description

Fig. 1 shows the ITPS panel that is studied, which is a corrugated core sandwich panel concept.

The design consists of a top face sheet and webs made up of titanium alloy (Ti–6Al–4V), and a bottom face sheet made up of beryllium. Saffil® foam is used as insulation between the webs. The relevant geometric variables of the ITPS design are also shown on the unit cell in Fig. 1. These variables are the top face thickness (t_T), bottom face thickness (t_B), thickness of the foam (d_S), web thickness (t_w), corrugation angle (θ), and length of unit cell ($2p$). The mass per unit area is calculated using the below equation:

$$m = \rho_T t_T + \rho_B t_B + \frac{\rho_w t_w d_S}{p \sin \theta} \tag{1}$$

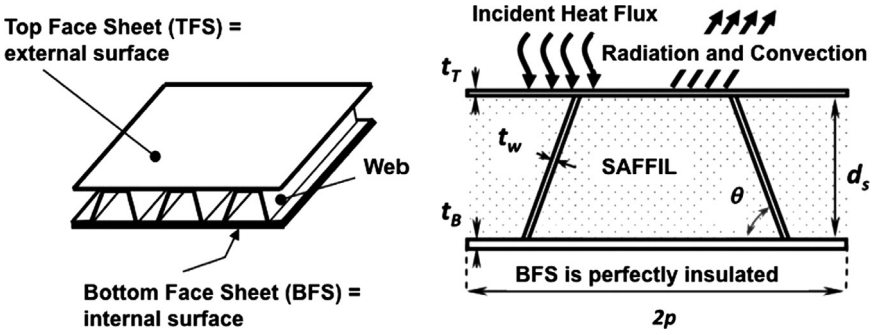

Fig. 1. Corrugated core sandwich panel ITPS concept.

where ρ_T, ρ_B, and ρ_w are the densities of the materials that make up the top face sheet, bottom face sheet, and web, respectively. Additional information on the integrated thermal protection system is provided in Appendix A.

In this study, we consider thermal failure to occur when the temperature of the bottom face sheet exceeds an allowable temperature. We assume that tests of the structure will be conducted to verify the design. Observed data from the test will be utilized to calibrate errors in analytical calculations.

3. Analysis and post-design test with redesign

It is assumed that an analyst has a computational model by which to calculate the change in the temperature of the bottom face sheet of the ITPS, ΔT_{calc}, for a design described by design variables d and random variables r. The randomness is due to variabilities in material properties, manufacturing, and environmental effects. Using ΔT_{calc}, the calculated temperature is defined as

$$T_{calc}(d,r,v_0) = T_0(1-v_0) + \Delta T_{calc}(d,r) \tag{2}$$

where T_0 is the initial temperature of the bottom face sheet, which also has variability represented by v_0. Note that Eq. (2) is formulated in such a way that the magnitude of the variability is dependent on T_0, such that $T_0(1-v_0) = T_0 - T_0 v_0$ as opposed to defining T_0 with variability as $T_0 - v_0$. T_0 itself is a deterministic value, and we chose this formulation in order to keep it consistent with the formulation of errors and to prevent v_0 from being on the order of magnitude of the temperature.

The design is obtained via a deterministic optimization problem which requires that the calculated temperature be less than or equal to some deterministic allowable temperature T^{det}_{allow} by a safety margin S_{ini} as shown in Eq. (3). Traditionally, the value of this safety margin is determined by regulations and past experience:

$$\min_{d=\{t_w,t_B,d_S\}} \quad m(d) \tag{3}$$

$$\begin{aligned} \text{subject to} \quad & T_0 + \Delta T_{calc}(d, r_{nom}) + S_{ini} \le T^{det}_{allow} \\ & t_{w,L} \le t_w \le t_{w,U} \\ & t_{B,L} \le t_B \le t_{B,U} \\ & d_{S,L} \le d_S \le d_{S,U} \end{aligned} \tag{4}$$

Note that for the deterministic design, the random variables are held at the nominal value r_{nom} and the variability in the initial temperature is zero. The subscripts L and U on the design variables represent the lower and upper bounds, respectively. The solution of the optimization problem is denoted as d^*_{ini}.

After the design stage, a test is conducted to verify the chosen design. The test is performed on a test article described by d_{test} (possibly slightly different than d^*_{ini} due to manufacturing tolerances) and r_{test},[1] and an experimentally measured change in temperature, ΔT_{meas}, is found. For this test design, $\Delta T_{calc}(d_{test}, r_{test})$ and $T_{calc}(d_{test}, r_{test})$ are also calculated.

As a means of calibration, the experimentally measured and calculated temperatures can be used in the form of a correction factor θ for the computational model. That is, the corrected calculated temperature is given as

$$\begin{aligned} & T_{calc,corr}(d,r,v_0) = T_0(1-v_0) + \theta \Delta T_{calc}(d,r) \\ & \text{where } \theta = \frac{\Delta T_{meas}}{\Delta T_{calc(d_{test},r_{test})}} \end{aligned} \tag{5}$$

[1] It is assumed that the test article design is accurately measured such that both d_{test} and r_{test} are known, and there is no variability in the initial temperature.

Note that this results in an updated distribution of the corrected-calculated temperature.

Should the test result show that a design is unacceptable, redesign occurs. The criterion for redesign is based on the safety margin of the corrected calculated temperature of the original design. The lower and upper limits of the safety margin of the corrected temperature are represented with S_L and S_U, respectively. This is expressed as

$$\begin{aligned} & \text{Redesign if : } \; S_{corr} = T^{det}_{allow} - (T_0 + \theta \Delta T_{calc}(d^*_{ini}, r_{nom})) < S_L \\ & \quad \text{or } S_{corr} = T^{det}_{allow} - (T_0 + \theta \Delta T_{calc}(d^*_{ini}, r_{nom})) > S_U \end{aligned} \tag{6}$$

Deterministic redesign is performed so that the corrected calculated temperature of the redesign (with the correction factor) is less than or equal to the allowable temperature by a safety margin S_{re}. This safety margin S_{re} does not necessarily need to be equal to the initial safety margin S_{ini}. Since more information is gained from the test, the designer may choose to design to save weight by reducing the safety margin. This can be formulated into an optimization problem to minimize the mass given a constraint on the corrected calculated temperature of the new redesign, where the design variables are the geometry

$$\begin{aligned} \min_{d=\{t_w,t_B,d_S\}} \quad & m(d) \text{subject to} \quad T_0 + \theta \Delta T_{calc}(d, r_{nom})_{re} + S_{re} \le T^{det}_{allow} \\ & t_{w,L} \le t_w \le t_{w,U} \\ & t_{B,L} \le t_B \le t_{B,U} \\ & d_{S,L} \le d_S \le d_{S,U} \end{aligned} \tag{7}$$

The optimum updated design is denoted d^*_{upd}.

4. Uncertainty definition

Oberkampf et al. [17] provided an analysis of different sources of uncertainty in engineering modeling and simulation, which was simplified by Acar et al. [5]. We use classification similar to Acar's to categorize types of uncertainty as errors (uncertainties that apply equally to every ITPS) or variability (uncertainties that vary in each individual ITPS). We further describe errors as epistemic and variability as aleatory. As described by Rao et al. [18], the separation of the uncertainty into aleatory and epistemic uncertainties allows more understanding of what is needed to reduce the uncertainty (i.e., using tests to gain more knowledge thereby reducing the error), and trade off the value of the information needed to reduce the uncertainty against the cost of the reduction of the uncertainty.

Variability is modeled as random uncertainties that can be modeled probabilistically. We simulate the variability through a Monte Carlo simulation (MCS) that generates values of the random variables r based on an estimated distribution and calculates the change in bottom face sheet temperature ΔT_{calc}. In addition, we sample the variability v_0 in the initial temperature. This forms the temperature T_{calc} for each sample, generating the probability distribution function. The calculated temperature distribution that reflects the random variability is denoted $f_{calc}(T)$. Additionally, we have variability in the allowable temperature T_{allow}.

In contrast to variability, errors are fixed for a given ITPS and the true values are largely unknown, so they can be modeled probabilistically as well. We have classified two sources of error, which are described in Table 1.

In estimating the temperature of a design, the error must also be considered. As previously described, the calculated temperature distribution $f_{calc}(T)$ of the design reflects random variability. If the true value of the computational error is known, then the true temperature distribution, $f_{true}(T)$, associated with $f_{calc}(T)$ is known,

Table 1
Description of errors.

Symbol	Description
e_c	Computational error due to modeling of the temperature change ΔT_{calc}
e_x	Experimental error in measuring ΔT_{meas}

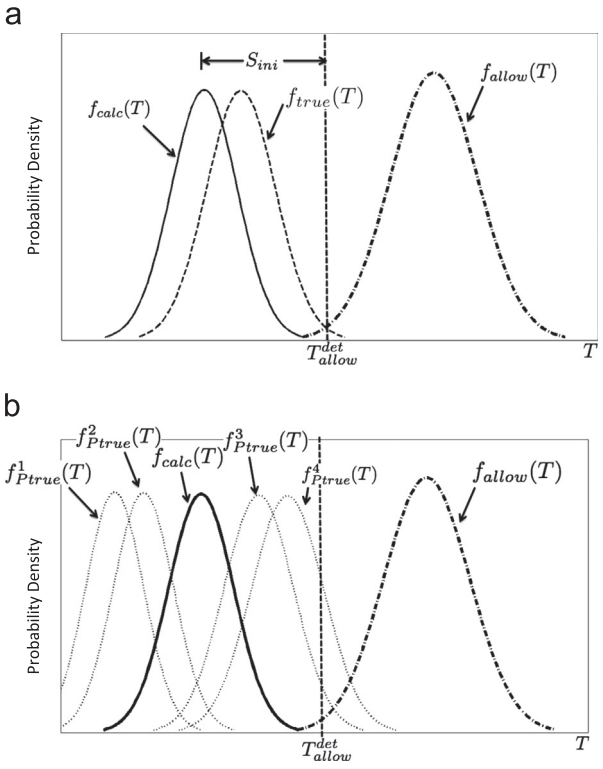

Fig. 2. Example illustrating (a) known calculated and allowable temperature distributions and unknown true distribution, (b) 4 possible true temperature distributions obtained by sampling of 4 values of e_c.

as shown in Fig. 2(a). The true temperature still has randomness due to the variabilities.

Since the error is unknown and modeled probabilistically, we instead sample the computational error to create several possible distributions of the true temperature distributions, $f^i_{Ptrue}(T)$ corresponding to the i th sample of e_c. This sampling is illustrated in Fig. 2(b) for 4 samples of e_c. Using the allowable temperature distribution, the probability of failure can be calculated for each sample of the computational error. This forms a distribution of the probability of failure, which is further described in the next section.

5. Distribution of the probability of failure

The true temperature for a design described by geometric design variables d and random variables r can be defined as

$$T_{true}(d,r,v_0) = T_0(1-v_0) + (1-e_{c,true})\Delta T_{calc}(d,r) \quad (8)$$

The limit state for the probability of failure takes into account the variability in the allowable temperature[2] along with the distribution of the true temperature. The limit state equation is formulated as the difference between a capacity C and response R as shown in the below equation:

$$g_{true} = T_{allow} - T_{true}(d,r,v_0) = C - R \quad (9)$$

Using the limit state equation, the probability of failure is calculated using Separable Monte Carlo [19]. The probability of failure p_f is calculated with Eq. (10), where M and N are the number of capacity and response samples, respectively. The indicator function I is 1 if the g is less than zero and 0 otherwise

$$p_f = \frac{1}{MN}\sum_{i=1}^{N}\sum_{j=1}^{M} I[g_{true}(C_j,R_i) < 0] \quad (10)$$

As described in the previous section, a distribution of the probability of failure can be formed by sampling the computational error for $e_{c,true}$ and calculating the probability of failure for each sample. Therefore, for n samples of $e_{c,true}$ there are n probability distributions $f_{true}(T)$ from which we can calculate n p_f values. Recall that each sample represents a possible future for the design. From these n values, we can calculate the mean and 95th percentile of the probability of failure. The following section will describe this process of sampling the errors to simulate the future alternatives.

6. Simulating future processes at the design stage

Monte Carlo sampling of the true values of the computational and experimental errors from the assumed error distributions is used to simulate the future test and redesign alternatives for the initial optimum design d^*_{ini}. The steps to simulate a single alternative of the future test with possible redesign are listed below:

1. Sample set of errors e_c and e_x from assumed distributions (from this, the "before redesign" probability of failure using the e_c sample can be calculated).
2. Use the true e_c and e_x samples to simulate a test result and correction factor θ (Eq. (5) with further details in Appendix B).
3. Apply the correction factor based on the test result to ΔT_{calc} (Eq. (5)).
4. Calculate the safety margin with the corrected temperature and evaluate if redesign is necessary based on S_L and S_U (Eq. (6)), then redesign, if necessary (Eq. (7)).
5. If redesign took place, calculate the mass and probability of failure for this alternative.

To simulate another alternative future, the true errors are resampled and the process is repeated. For n possible future alternatives, we sample n sets of the errors, and obtain n true probabilities of failure and up to n updated designs (with n mass values). With these n values, we can calculate the mean and 95th percentile of the probability of failure and mass. In how many futures we will need to redesign is determined by the window defined by S_L, S_U. If a redesign is needed, the updated design will be determined by the choice of safety margin S_{re} required in redesign. Fig. 3 illustrates how the distribution of $T_{calc,corr}$, probability of failure, and mass changes with redesign for a given S_{ini}, S_{re}, S_L, and S_U for n alternative futures.

If the choice of the safety margin and redesign window leads to k redesigns, the probability of redesign p_{re} is

$$p_{re} = \frac{k}{n} \times 100\% \quad (11)$$

Fig. 4 displays the above process, and the calculation of the mean mass, mean probability of failure, and 95th percentile of the probability of failure of a candidate design, for n alternative futures.

[2] The absence of the superscript "det" for T_{allow} denotes the allowable temperature with variability to distinguish it from the deterministic allowable temperature T^{det}_{allow}.

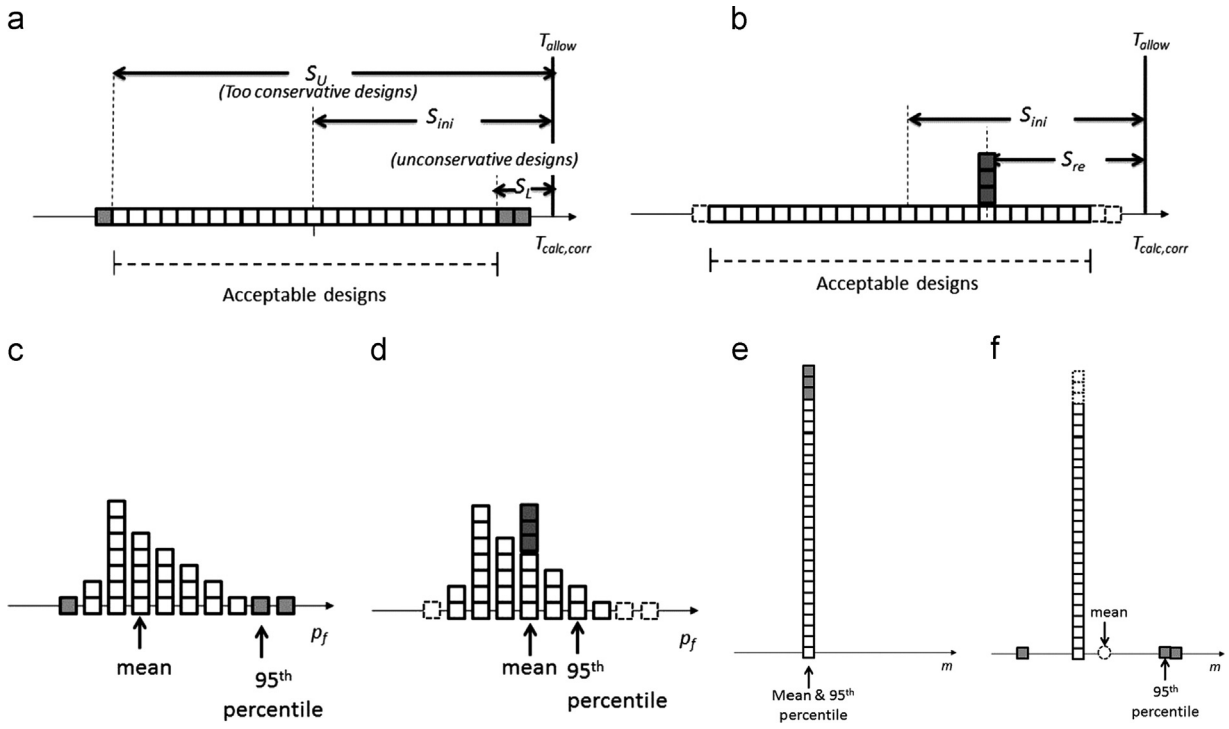

Fig. 3. Illustrative example of before and after redesign distributions of (a) and (b) $T_{calc,corr}$, (c) and (d) probability of failure, and (e) and (f) mass for n alternative futures for a given S_{ini}, S_{re}, S_L, and S_U.

In this figure, a test is performed from which the correction factor θ is obtained. The corrected safety margin is then used to determine if redesign should be performed based on the redesign criterion. If redesign is required, then the design given the redesign safety margin is found, and the mass and probability of failure are calculated. Otherwise, the original mass of the design and probability of failure is calculated. After this is repeated for the n alternatives (i.e., n θ values), the mean mass, mean probability of failure, and 95th percentile of the probability of failure can be calculated.

7. Optimization of the safety margins and redesign criterion

7.1. Problem description

The process shown in Fig. 4 can be thought of as the process that is used by a designer in the design of an ITPS with a given set of safety margins (S_{ini} and S_{re}) and redesign criterion (S_L and S_U), leading to a distribution of the future mass and probability of failure. In this section, we explore how a company may use the probability of failure with future redesign to choose the safety margins and redesign criterion to minimize mass and probability of redesign. To do this, we formulate an optimization problem that minimizes the mean mass μ_m and probability of redesign p_{re} subject to constraints on the future mean probability of failure μ_{p_f}, and the 95th percentile of the probability of failure $P_{95}(p_f)$. The design variables are the safety margins and redesign criterion. The formulation is shown in the below equation:

$$\begin{aligned}
&\min_{S_{ini},S_L,S_U,S_{re}} \quad \mu_m, p_{re}\\
&\text{subject to} \quad (\mu_{p_f})_{Before\ Redesign} \le 0.1\%\\
&\quad (P_{95}(p_f))_{Before\ Redesign} \le 0.5\%\\
&\quad (\mu_{p_f})_{After\ Redesign} \le 0.01\%\\
&\quad (P_{95}(p_f))_{After\ Redesign} \le 0.05\%
\end{aligned}$$

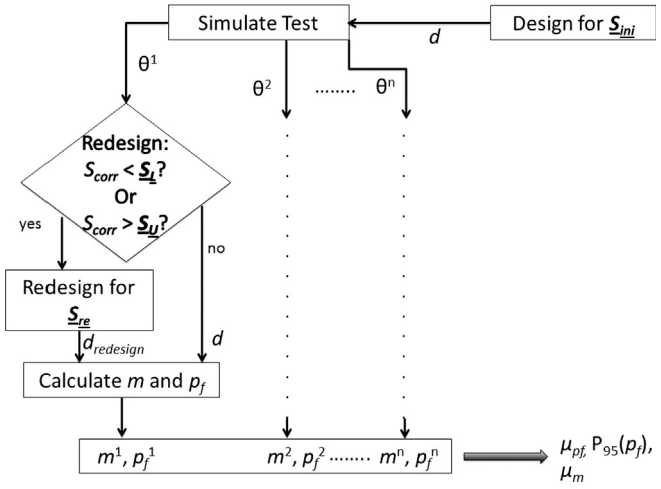

Fig. 4. Flowchart of the process to calculate the mean mass, mean probability of failure, and 95th percentile of the probability of failure for a candidate design that satisfies the problem in Eq. (11) for n future alternatives. Note that the design variables are underlined to show their position in the process.

$$\begin{aligned}
&35 \le S_{ini},\ S_{re} \le 65\\
&S_{ini} - 35 \le S_L \le S_{ini}\\
&S_{ini} \le S_U \le S_{ini} + 35\\
&1.24\ \text{mm} \le t_w \le 1.77\ \text{mm}\\
&4.94\ \text{mm} \le t_B \le 7.06\ \text{mm}\\
&49.9\ \text{mm} \le d_S \le 71.3\ \text{mm}
\end{aligned} \tag{12}$$

The constraints on S_{ini} and S_{re} restrict the two values to be within the window of 35–65 K, and they are not constrained to have equal values. The lower limit is intended to reflect a regulatory mandate, but, just in case, bounds on the before redesign probability of failure are present to prevent designs that are largely unsafe before redesign. The constraints on S_L and S_U

Table 2
Bounds of computational and experimental errors.

Error	Distribution	Bounds
e_c	Uniform	± 0.12
e_x	Uniform	± 0.03

restrict the acceptable values of the safety margin after correction to within 35 K of S_{ini}. Note that in this paper the design and redesign policy is optimized on the basis of a single panel. If an optimization like that is carried out in practice, we assume that compromise values will be used based on similar optimizations for several cases. For this problem, the computational and experimental errors were distributed as described in Table 2. We have made the assumption that the engineer has some prior experience and history with similar models that allow him or her to make an estimate of the error distributions. Clearly, this estimate will not be accurate, but we assume that the estimated distribution of errors is conservative. The engineer may also be able to evaluate more accurate but costly higher fidelity models at certain design points for the purpose of estimating the error bounds. Given the distributions of the errors, the correction factor θ ranged from 0.85 to 1.15. The distributions of the variables with uncertainty due to variability are provided in Appendix A.

In this work, the computational model was a finite element model built in Abaqus for which transient analysis was used to determine the change in the maximum bottom face sheet temperature. However, coupling the time consuming transient analysis with the Monte Carlo simulations needed to obtain probabilities of failure over alternative futures was not tractable. Therefore, Abaqus simulations were fitted with quadratic response surfaces, originally described in [20]. The simulations were performed at a set of points determined by Latin Hypercube sampling of 180 designs. A quadratic response surface of 15 variables of the change in maximum bottom face sheet temperature was developed. The reader is referred to Appendix A for further details on the creation of the surrogate for the computational model.

To further reduce the computational cost of simulating a future test, surrogates of the mass and reliability index were developed. The reliability index β is related to the probability of failure by $p_f = \Phi(-\beta)$, where Φ is the standard normal cumulative density function. For example, for a probability of failure of 0.1%, the reliability index is 3.72. For the points that were used to form the surrogate of the reliability index, Separable Monte Carlo (SMC) was used to calculate the probability of failure. The accuracy of the Separable Monte Carlo prediction of probability of failure was estimated by bootstrapping. In this work, 10,000 samples of the response and capacity were used. To estimate the standard deviation, the response and capacity were separately sampled with replacement to have 10,000 samples of response and capacity, and the probability of failure was calculated. The number of bootstrap repetitions was 1000. For this work, we desired a coefficient of variation less than or equal to 0.1. For 10,000 samples, we determined that for a design with a probability of failure of 1e−3, which is on the order of probabilities of failure examined in this study, the standard deviation was 1e−4 for a coefficient of variation of 0.1. The development of these surrogates is described in Appendix C.

The problem in Eq. (11) was solved by forming a cloud of 10,000 points using Latin Hypercube sampling of the design variables S_{ini}, S_L, S_U, and S_{re}. For each set of design variables, 10,000 alternative futures were sampled to obtain the probability of redesign and distributions of the mass and probability of failure. The selection of $n=10{,}000$ was chosen in order to have a coefficient of variation of the probability of redesign less than or equal to 0.1 for a probability of redesign of 1% as probability of redesign ranged from 1% to 50%. The coefficient of variation was estimated by $\sqrt{(1-p_{re})/p_{re}n}$. For $n=10{,}000$, the coefficient of variation for $p_{re}=0.01$ was 0.0995 for a standard deviation of 9.95e−4.

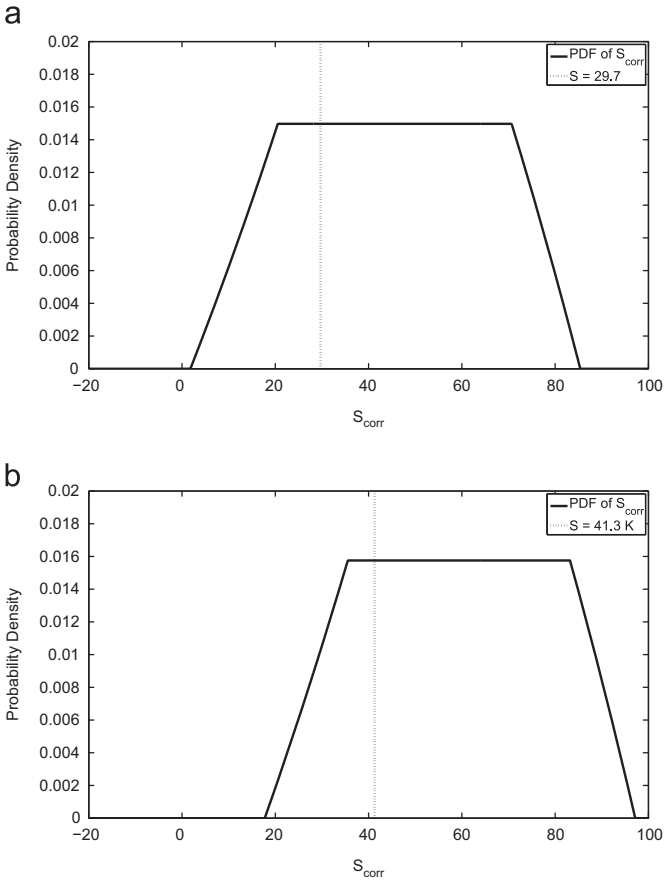

Fig. 5. Probability density function of the safety margin after correction for (a) $S_{ini}=48.9$ K which also displays the S_{ini} required in the absence of epistemic uncertainty for a mass of 23.9 kg/m^2 and (b) $S_{ini}=62.5$ K which also displays the S_{ini} required in the absence of epistemic uncertainty for a mass of 24.3 kg/m^2.

7.2. Results

As a point of comparison, we first found the optimum design for minimum mass that satisfied the "before redesign" constraints on the probability of failure. Since redesign was not performed, the only value of interest is S_{ini}. The minimum value of $S_{ini}=48.9$ K which satisfied the probability constraints of a mean of 0.1% and 95th percentile of 0.5% led to a mass of 24.7 kg/m^2. In addition, we found the minimum S_{ini} design that satisfied the "after redesign" probability of failure constraints without actually performing redesign (i.e., the minimum S_{ini} that satisfied $\mu_{p_f} \le 0.01\%$ and $P_{95}(p_f) \le 0.05\%$ without any redesign). In this case, the minimum S_{ini} was 62.5 K for a mass of 25.3 kg/m^3 for $\mu_{p_f}=0.01\%$ and $P_{95}(p_f)=0.05\%$. Plots of the probability density of the safety margin after correction (i.e., $S_{corr}=T_{allow}-T_{calc,corr}$) for the $S_{ini}=48.9$ K and $S_{ini}=62.5$ K cases are shown in Fig. 5.

Fig. 5 shows the distribution of the corrected safety margins with the two values of S_{ini}. The figure also shows the value of S needed to achieve the desired probabilities of failure ($S_{ini}=29.7$ K for $\mu_{p_f}=0.1\%$ in Fig. 5(a) and $S_{ini}=41.3$ K for $\mu_{p_f}=0.01\%$ in Fig. 5 (b)) in the absence of epistemic uncertainty. We observed that 79% of S_{corr} values were greater than 29.7 K for $S_{ini}=48.9$ K and 84%

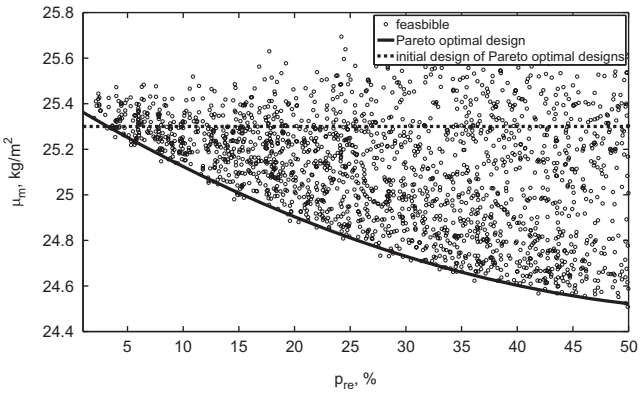

Fig. 6. Pareto front for minimum probability of redesign and mean mass after redesign. Feasible points in the design space are shown, along with the before-redesign mass of the points on the Pareto front.

greater than 62.5 K for $S_{ini} = 41.3$ K. This was because the mean probability of failure was influenced disproportionately by a few large values as the median probability of failure before redesign was 7.3e−4% for $S_{ini} = 48.9$ K and 3.2e−6% for $S_{ini} = 62.5$ K. The figure caption also notes that the mass required to achieve the desired probability of failure in the absence of epistemic uncertainties was 23.9 kg/m^2 for 0.1% and 24.3 kg/m^2 for 0.01%. With the epistemic uncertainty, we required 25.3 kg/m^2 to compensate for the computational error, and this 1 kg/m^2 or 4% penalty was what can be reduced by more accurate computation or tests.

Allowing redesign, the Pareto front for minimum probability of redesign and mean mass after redesign is displayed in Fig. 6 that satisfies the constraints of the problem in Eq. (11). We observed reductions in mean mass with increasing probabilities of redesign. The mean mass values after redesign at these points were less than the minimum mass of 25.3 kg/m^3 obtained when redesign was not allowed. At 40% probability of redesign, the mean mass was even less than 24.7 kg/m^3, the mass of the optimum design that satisfied the relaxed "before redesign" constraints on probability of failure ($\mu_{p_f} \leq 0.1\%$ and $P_{95}(p_f) \leq 0.5\%$).

The values of the safety margins for the designs on the Pareto front are displayed in Fig. 7. We observed that the initial safety margin S_{ini} was nearly constant at approximately 63 K. The lower bound of the acceptable safety margin with correction S_L remained between 28 and 32 K, for which the difference from S_{ini} is near the upper bound of 35 K (i.e., the constraint on the lower bound of S_L is active or nearly active). This resulted in the small probability of redesign of unconservative designs. In Fig. 8, which shows the percentage of the total probability of redesign that is conservative and unconservative, we observed that this was indeed the case, and that less than 5% of the total probability of redesign was attributed to unconservative redesign for all points on the Pareto front.

For the upper bound on acceptable safety margin with correction S_U, we observed that the values were large (nearly 100 K) but gradually reduced to values near S_{ini} at 65 K. This led to the gradual increase in probability of conservative redesign as the probability of unconservative redesign remained at low values. Thus, the probability of conservative redesign comprised the majority of the total probability of redesign for the designs on the Pareto front. At the same time, we observed that the safety margin S_{re} of the redesign was set to values below S_{ini} and at values less than the minimum value without tests and redesign of 63.5 K. That is, after the test, the redesign has a smaller safety margin than possible for the original design. This value is even less than the safety margin required to satisfy the relaxed before redesign constraints of $S_{ini} = 48.9$ K. The combined effect of redesigning conservative

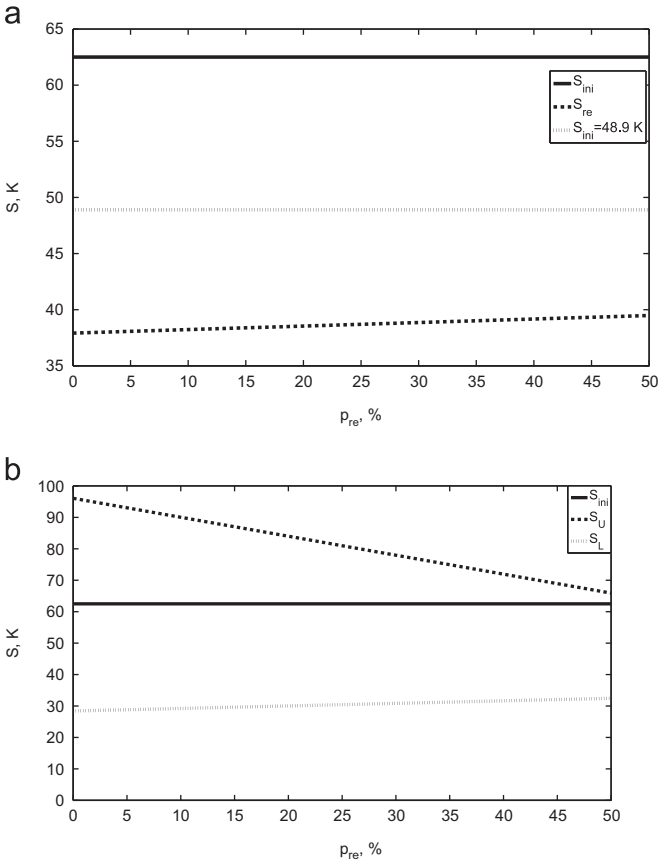

Fig. 7. For Pareto front for minimum probability of redesign and mean mass after redesign, (a) initial and redesign safety margins versus total probability of redesign and (b) bounds of the acceptable corrected safety margins versus total probability of redesign.

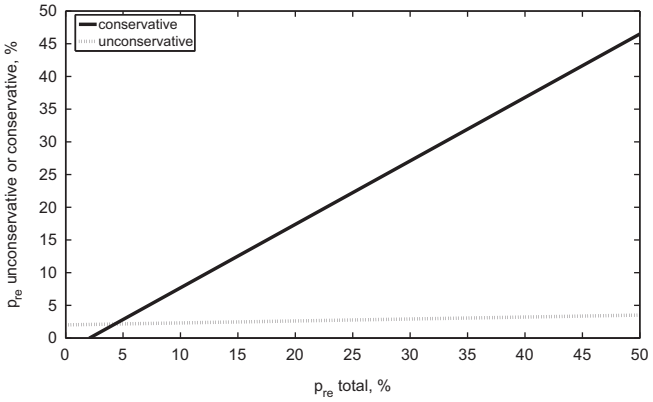

Fig. 8. Percentage of conservative and unconservative redesigns of the points on the Pareto front.

designs for a reduced safety margin was a reduction in the mean mass while satisfying more stringent constraints on the probability of failure.

The results show that the optimal choice safety margins and redesign criterion can be chosen based on the probability of failure that accounts for future redesign. We observe that companies can benefit by having designers consider conservative safety margins for the initial design, which correspond to the safety margin required to satisfy the probabilistic constraints. The redesign criterion should then mostly result in the redesign of overly conservative designs to trim mass by allowing a smaller safety

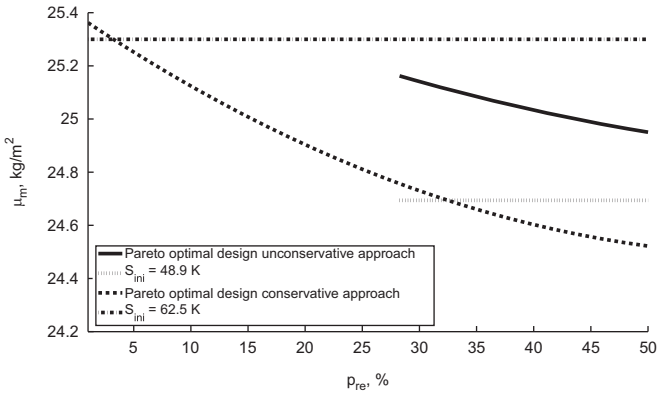

Fig. 9. Pareto front showing the Pareto front found for the unconservative approach (with $S_{ini} = 48.9$ K) in comparison to the Pareto front with the conservative approach (with $S_{ini} = 62.5$ K).

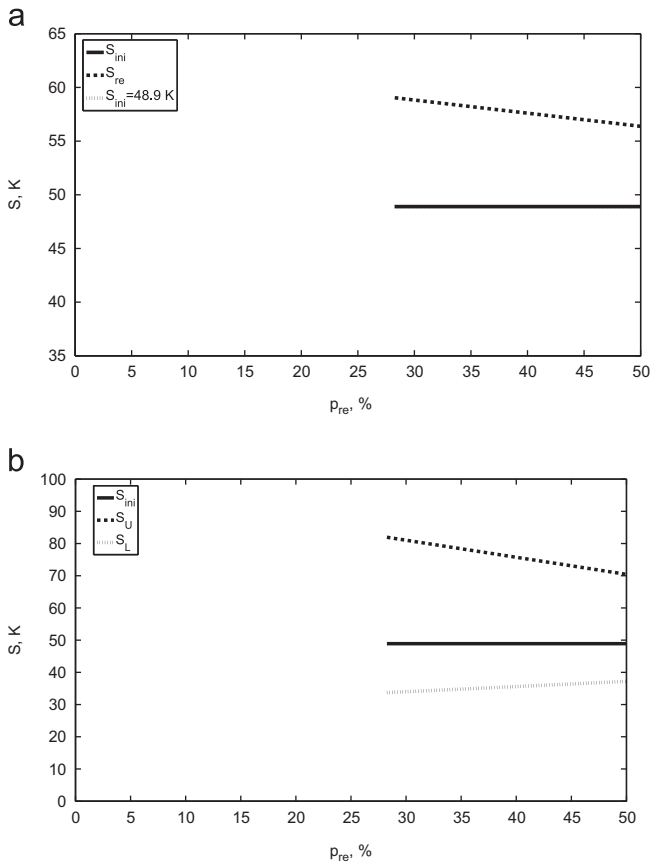

Fig. 10. For Pareto front for minimum probability of redesign and mean mass after redesign with the unconservative-first approach, (a) initial and redesign safety margins versus total probability of redesign and (b) bounds of the acceptable corrected safety margins versus total probability of redesign. Note that for (c) the lines for S_{ini} and $S_{ini} = 48.9$ K overlap.

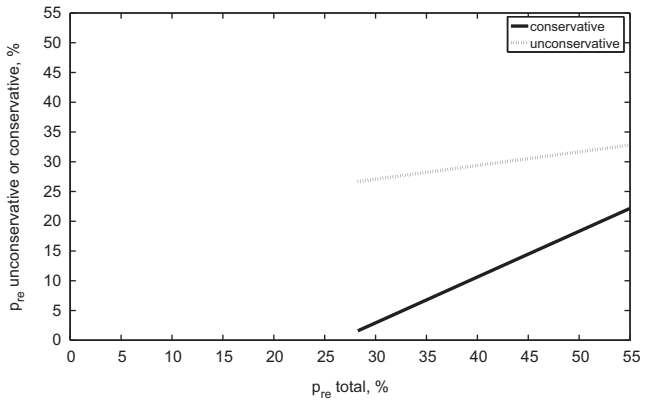

Fig. 11. Percentage of conservative and unconservative redesigns of the points on the Pareto front with the unconservative-first approach.

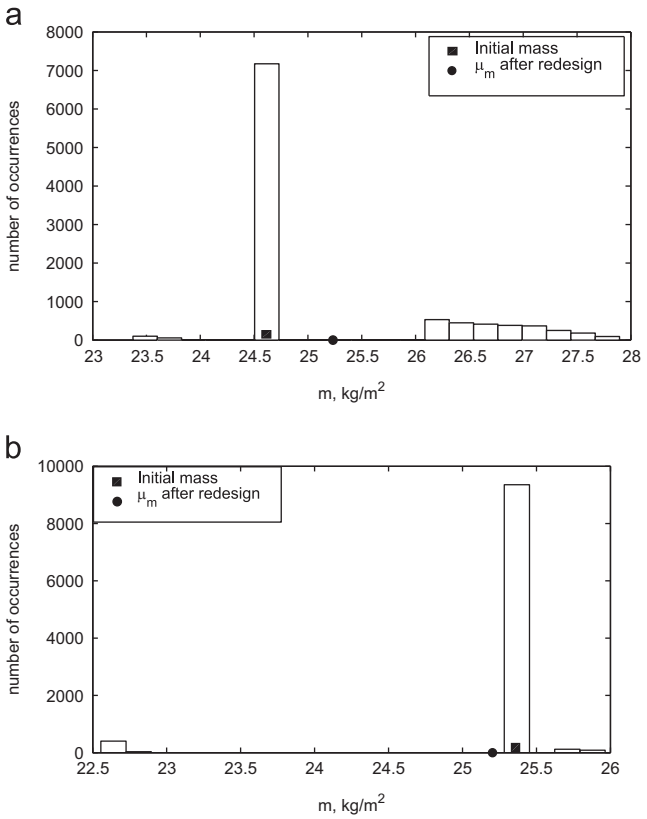

Fig. 12. Histograms of mass after redesign for 10,000 alternative futures for (a) initially unconservative design with 27% probability of redesign and (b) initially conservative design with 8% probability of redesign.

margin for redesign (because of additional knowledge due to the test in the correction factor), with a few unsafe designs redesigned for safety.

7.3. Unconservative initial design approach

While the Pareto optimal designs showed that the initial design should be conservative with redesign performed to trim mass, we examined the trade-off in probability of redesign and mass when starting with an initially unconservative design (i.e., an initial design that does not satisfy the constraints of p_f). In this approach, the designer uses a smaller safety margin to achieve a minimal weight design, relying on the test and redesign to correct any dangerous designs. In this problem, the initial safety margin was fixed at 48.9 K (corresponding to a mass of 24.7 kg/m^2) and the remaining safety margins (S_{re}, S_L, and S_U) were the design variables. The same constraints as in Eq. (12) were used. Fig. 9 displays the Pareto front found with the unconservative approach, and compares the result to the previously found results that used a conservative-first approach found in Section 7.2.

It was observed that to meet the probability of failure requirements, the probability of redesign was at least 27% for the unconservative approach with $S_{ini} = 48.9$ K. That is, the designer must accept at least a 27% probability of redesign, which would

Table 3
Breakdown of alternative futures for the unconservative initial design with 27% probability of redesign and conservative initial design with 8% probability of redesign.

Outcome	p_{re} (%)	Mean mass (kg/m^2)
Initially unconservative		
No redesign	73	24.7
Unconservative	25.5	26.8
Conservative	1.5	23.5
Total		25.2[a]
Initially conservative		
No redesign	93.5	25.3
Unconservative	2.1	25.8
Conservative	4.4	22.7
Total		25.2[a]

[a] Calculated as $p_{noredesign}m_0+(p_{re}\mu_m)_{conservative}+(p_{re}\mu_m)_{unconservative}$.

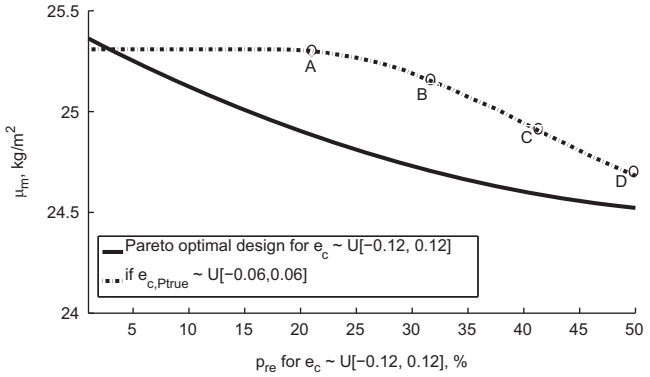

Fig. 13. Comparison of the points on the Pareto front for e_c between ± 0.12 when the error is actually between ± 0.06 (c.f. Fig. 6). The comparison of the points marked A, B, C, and D is provided in Table 4.

lead to a mean mass of approximately 25.2 kg/m^2. This value of the mass is only 0.4% smaller than the initial mass required to satisfy the probability constraints without redesign with the initially conservative design.

Fig. 10 displays the values of the design variables of the Pareto optimal solutions, and Fig. 11 displays the breakdown of the total probability of redesign due to conservative and unconservative designs. It was observed that redesign was primarily performed to increase safety at the smallest probabilities of redesign (27%), increasing the redesign of conservative designs with increasing probability of redesign.

The histogram of the mass for 10,000 alternative futures after redesign is displayed in Fig. 12(a). The approximately 2% increase in the mean mass after redesign is attributed to the large probabilities of failure associated with redesign of unconservative designs. A breakdown of the alternative futures that resulted in the mean mass is shown in Table 3. It was observed that the redesign of unconservative designs resulted in an increase of 8% in the mean mass.

In contrast, the same mean mass of 25.2 kg/m^2 after redesign can be achieved with the conservative-first approach with a probability of redesign around 8%, and for a probability of redesign of 27%, the mean mass is nearly 24.7 kg/m^2. In this case, the reduction in mean mass is due to large reductions in mass in the cases that required redesign of conservative designs. The histogram of the mass for 10,000 alternative futures is shown in Fig. 12(b) and the mass and probability of redesign are detailed in Table 3. It was observed that the redesign of overly conservative designs resulted in a 10% reduction in the mean mass. Comparing this value along with the 8% increase in mass seen in the initially

Table 4
Comparison of predicted and actual probability of redesign and mass reduction for points on Pareto front when e_c is estimated between ± 0.12 when it is actually between ± 0.06.

Point	p_{re} (%)		μ_m reduction (kg/m^2)	
	Predicted	Actual	Predicted	Actual
A	20	0.3	0.51	0.09
B	30	6.1	0.65	0.19
C	40	22	0.80	0.49
D	50	40	0.88	0.72

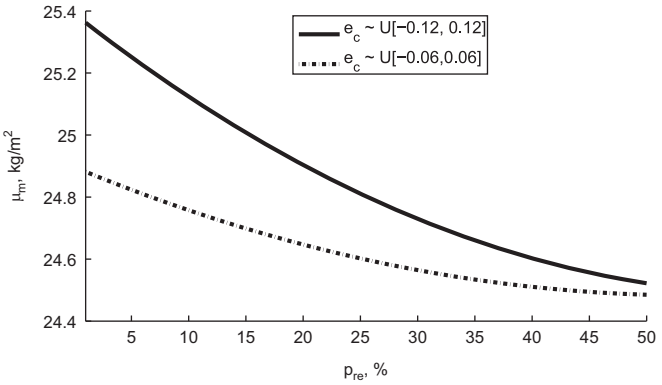

Fig. 14. Comparing the points on the Pareto optima front for e_c between ± 0.06.

unconservative case, we observed that the change in mass due to redesign is much larger than the 2% difference in mass of the two initial designs. However, with the initially conservative design most redesigns act to reduce the mass, whereas the mass is mostly increased in the initially unconservative redesign cases. Therefore, the designer has a choice:

1. use a smaller initial safety margin for an initially small mass and accept a 27% probability of redesign that will increase the mass, or
2. use a larger initial safety margin for an initially larger mass that can achieve less than or equal to the same mass with probabilities of redesign greater than 8%.

If the test shows that the component does not have to be redesigned, there would be a nearly 2% mass penalty in using the conservative safety margin.

7.4. Effect of excessively conservative computational error estimates

We also studied the effect of an excessively conservative computational error estimate. To do so, we set the distribution of e_c to be actually between ± 0.06 when we have estimated the error as between ± 0.12 and simulated 10,000 alternative futures with the smaller error for the points on the Pareto front for ± 0.12.

We first examined the penalty on the mass when overestimating the error as shown in Fig. 13. It was observed that, other than at very small probabilities of redesign, the mean mass was greater than predicted. Recall that the mass reduction with increasing redesign was due to redesign of mostly overly conservative designs to reduce the mass, and with smaller errors there is smaller gain from redesign. We compared the predicted and actual values of the probability of redesign and reduction in mass for four points on the Pareto front in Table 4. It was observed that the positive

aspect of the overly conservative error estimate was a smaller risk of redesign, but at the cost of a decreased mass reduction.

Next, we compared the Pareto front for e_c between ± 0.12 to the Pareto front found when it is instead between ± 0.06. This Pareto front was found in the same way as the Pareto front for e_c between ± 0.12 as described in Section 7.1. The comparison of the Pareto fronts is shown in Fig. 14. We observed that the difference between the two Pareto fronts was larger at smaller probabilities of redesign, with the difference gradually reducing with increasing probability of redesign. With a smaller computational error, the designer is able to reduce the mass of the design and, as before, use redesign of conservative designs to further reduce the mass.

Such a study that compares the effect of a smaller computational error distribution is useful to decide if measures should be taken to more accurately quantify the computational error or improve the model by increasing the fidelity, for example. The smaller mass for the case with the smaller error over the original Pareto front is a measure of the opportunity loss in not providing a better error estimate. For example, consider Point A in Fig. 13, where the designer expected to reduce the mass from 25.4 kg/m^2 to 24.9 kg/m^2 by tolerating a 20% probability of redesign. Fig. 13 and Table 4 show that instead the actual mass was 25.3 kg/m^2 with only a 0.3% probability of redesign. Fig. 14 shows that if the actual smaller error bounds were known, for the same 0.3% probability of redesign, the obtained mass after redesign would have been 24.87 kg/m^2. Such results are useful in providing an incentive to better estimate or reduce the computational error. For the opposite case, when the computational error is actually larger than estimated (e.g., if the true e_c was larger than ± 0.12 when we have estimated it as between those bounds), we expect that the test will catch such a scenario and the model itself would be significantly revised.

7.5. Discussion

Using the minimal safety margin for the initial design can be thought of as using safety margins given by regulatory agencies, which provide minimum values of safety margins and safety factors. For example, the Federal Aviation Administration has recommended minimum design and test factors for structures on reusable launch vehicles [21]. In this paper, the values of S_{ini} (and S_{re}) of 35 K may be the minimum value imposed by an agency, and the value of 48.9 K may be the current minimum value imposed by a company based on history or experience. The results presented in the paper show that a company may have an incentive to impose their own safety margins, and set the design and redesign rules to balance development costs. The results in Section 7.2 showed that probabilistic constraints can be satisfied by first using a conservative safety margin and accepting a risk of increased development cost through increased redesign to trim excess mass. This directly contrasts the approach of using minimal safety margin values and redesigning based on the test result to increase safety. Considering the possible future redesign and its cost allows the company to make better decisions at the design stage.

8. Concluding remarks and future work

In this paper, we used the modeling of future redesign to provide a way of balancing development costs (test and redesign costs) and performance (mass) by designing the design and redesign rules. We observed that the presence of epistemic uncertainty led to a mass penalty, which could be reduced by a test and redesign. Since deterministic design employing safety margins and safety factors is common practice in industry, we showed that safety margins and redesign criteria can be chosen using the probability of failure with future redesign. A study on an integrated thermal protection system showed that a minimum mass design that satisfied probabilistic constraints can be achieved by having an initially conservative design and a redesign criterion such that redesign is mainly performed on overly conservative designs to trim excess mass. In contrast, we examined the trade-off in starting with an initially small safety margin, which may be a minimum value recommended by a regulatory agency, and using the test and redesign to correct dangerous designs. Therefore, in this example, a company would have an incentive to use conservative safety margins at the initial design stage, while increasing performance by implementing a redesign criterion aimed at discovering overly conservative designs. This also provides a balance between probabilistic design and the more traditional deterministic approach.

Additionally, this research addresses handling the cost of evaluating the response of the ITPS by creating accurate surrogates of the system response. The same approach is applicable to other complex systems as long as the number of design variables is not too high.

Future work includes considering the uncertainty reduction methods that often take place after a component is designed but before a component is tested. For example, lower fidelity methods may be used to find a starting point for the initial design. Before a design is tested, it may be better characterized through higher fidelity modeling or optimization in a smaller design space about this design. Both the higher fidelity modeling and re-optimization can reduce the uncertainty in the design before a test is even performed. Therefore, a study that models these actions and considers the subsequent uncertainty reduction would be useful in finding the optimal balance in design and development costs and performance. Additional future work includes incorporating the “buffered probability of failure” as a reliability measure as a robust substitute for probability of failure, as explained by Rockafellar and Royset [22].

Acknowledgments

The material is based upon work supported by NASA under Award no. NNX08AB40A and the Air Force Office of Scientific Research under Award FA9550-11-1-0066. Any opinions, findings, and conclusions or recommendations expressed in this material are those of the author(s) and do not necessarily reflect the views of the National Aeronautics and Space Administration or the Air Force Office of Scientific Research.

Appendix A. Integrated thermal protection system

Thermal analysis of the integrated thermal protection system is done using 1-D heat transfer equations on a model of the unit cell. The heat flux incident on the top face sheet of the panel is highly dependent on the vehicle shape as well as the vehicle's trajectory. As in previous studies reported by Bapanapalli [23] (Chapter 3, pp. 49–61), incident heat flux on a Space Shuttle-like vehicle was used. A large portion of the heat is radiated out to the ambient by the top face sheet, and the remaining portion is conducted into the ITPS. We consider the worst-case scenario where the bottom face sheet cannot dissipate heat by assuming the bottom face sheet is perfectly insulated. Also, there is no lateral heat flow out of the unit cell, so that heat flux on the unit cell is absorbed by that unit cell only. For a more in-depth description of the model and boundary conditions, the reader is referred to the Bapanapalli reference.

Table A1
ITPS random variables.

Variable	Distribution	Nominal	CV or σ
Web thickness	Uniform	–	CV=3%
Bottom face sheet	Uniform	–	CV=3%
Foam thickness	Uniform	–	CV=3%
Top face sheet thickness	Uniform	1.2 mm	CV=3%
Half unit cell length	Uniform	34.1 mm	CV=3%
Angle of corrugation	Uniform	80°	CV=3%
Density of titanium	Normal	4429 kg/m^3	CV=2.89%
Thermal conductivity of titanium	Normal	7.6 Wm/K	CV=2.89%
Specific heat of titanium	Normal	564 Jkg/K	CV=2.89%
Density of beryllium	Normal	1850 kg/m^3	CV=2.89%
Thermal conductivity of beryllium	Normal	203 W/m/K	CV=3.66%
Specific heat of beryllium	Normal	1875 J/kg/K	CV=2.89%
Density of foam	Normal	24 kg/m^3	CV=5.78%
Thermal conductivity of foam	Normal	0.105 W/m/K	CV=5.78%
Specific heat of foam	Normal	1120 J/kg/K	CV=2.89%
Initial temperature	Normal	0	$\sigma=0.01$
T_{allow}	Lognormal	660 K	CV=2.42%
T_{allow}^{det}	–	623.15 K	

Table A2
Correlated random variables.

Variable	Correlation coefficient
Density of titanium Thermal conductivity of titanium	0.95
Density of beryllium Thermal conductivity of beryllium	0.95
Density of foam Thermal conductivity of foam	0.95

Table A3
Goodness-of-fit statistics for the surrogate of the maximum bottom face sheet temperature.

Fit statistic	Value
R^2	0.99
$PRESS_{RMS}$	0.20%
e_{RMS}	0.07%

The random variables used in this paper are described in Table A1 (Table A2).

A surrogate of the maximum bottom face sheet temperature was originally constructed in [20]. The surrogate was a function of the first 15 variables in Table A1: 6 variables relating to the ITPS geometry and the remaining 9 as density, thermal conductivity, and specific heat of all three materials (titanium, beryllium, and insulation foam). A quadratic response surface was fitted to 180 training points from Latin Hypercube Sampling. Though a typical rule of thumb for the number of training points for a quadratic response surface is twice the number of coefficients (here, 136 coefficients), the number of training points was sufficient as evidenced by the goodness-of-fit statistics shown in Table A3. Note that the $PRESS_{RMS}$, found by leave-one-out cross-validation, and the e_{RMS} are reported as a percentage of the average value of the output of the training points. Due to the R^2 value near 1 and the small ($<1\%$) errors, the quadratic response surface was deemed an acceptably accurate surrogate.

Appendix B. Simulating a test result and correction factor θ

As described in Section 3, a test is performed to verify a design, and the test is performed on a test article denoted by d_{test} and r_{test} to find the experimentally measured temperature ΔT_{meas}. For this design, we can calculate $\Delta T_{calc}(d_{test}, r_{test})$. We can relate both the measured and calculated temperatures to the true temperature of the test article by the true experimental and computational errors as

$$\begin{aligned} T_{test,true} &= T_0 + \Delta T_{meas}(d_{test}, r_{test})(1-e_{x,true}) \\ &= T_0 + \Delta T_{calc}(d_{test}, r_{test})(1-e_{c,true}) \end{aligned} \tag{B.1}$$

Rearranging this equation, we arrive at the correction factor $\theta=(1-e_{c,true})/(1-e_{x,true})$.

Appendix C. Surrogates for mass and probability of failure

In this section, it is shown that the mass before and after redesign can be found using a surrogate that is a function of safety margin and difference between the allowable temperature T_{allow} and initial temperature T_0. A surrogate of the probability of failure that is a function of the same two variables and the computational error e_c can be made as well.

As shown in Eq. (3), the initial design satisfies

$$T_0 + \Delta T_{calc}(d,r) + S_1 = T_{allow} \tag{C.1}$$

Rearranged so that $\Delta T_{calc}(d,r)$ is on the left hand side, this becomes

$$\Delta T_{calc}(d,r) = (T_{allow} - T_0) - S_1 \tag{C.2}$$

By Eq. (7) the redesign should satisfy

$$T_0 + \theta \Delta T_{calc}(d,r) + S_4 = T_{allow} \tag{C.3}$$

which is rearranged so that $\Delta T_{calc}(d,r)$ is on the left hand side

$$\Delta T_{calc}(d,r) = (T_{allow} - T_0)/\theta - S_4/\theta \tag{C.4}$$

By Eqs. (C.2) and (C.4), the two are equivalent if $(T_{allow}-T_0) = [(T_{allow}-T_0)/\theta]_{afterredesign}$ and $S_1 = S_4/\theta$. Therefore, ΔT_{calc}, along with its corresponding mass and probability of failure, is a function of $(T_{allow}-T_0)$ and S, where the values with and without redesign are related through θ. This allows the mass to be calculated simply using surrogates with the inputs $(T_{allow}-T_0)$ and S. A surrogate to obtain the probability of failure can also be obtained by including the computational error e_c as an input.

Note that $\Delta T_{calc}(d,r)$ does not need to be calculated because, for a given $(T_{allow}-T_0)$ and S_1, we can find $\Delta T_{calc}(d,r)$ by

$$(T_{allow} - T_0) - S_1 = \Delta T_{calc}(d,r) \tag{C.5}$$

When the correction is applied, then we evaluate if redesign is necessary by

$$\begin{aligned} &\text{Redesign if : } (T_{allow}-T_0) - \theta[(T_{allow}-T_0) - S_1] \le S_2 \\ &\quad \text{or } (T_{allow}-T_0) - \theta[(T_{allow}-T_0) - S_1] \ge S_3 \end{aligned} \tag{C.6}$$

which simplifies to

$$\begin{aligned} &\text{Redesign if : } (T_{allow}-T_0)(1-\theta) + \theta S_1 \le S_2 \\ &\quad \text{or } (T_{allow}-T_0)(1-\theta) + \theta S_1 \ge S_3 \end{aligned} \tag{C.7}$$

Kriging surrogates (quadratic trend function with a Gaussian correlation model) were used for the surrogates of the mass and reliability index. The accuracy of the surrogates was measured by the $PRESS_{RMS}$, a leave-one-out cross validation error measure, and the e_{RMS} at 50 test points. A summary of the surrogates is provided in Table C1.

Appendix D. Effect of additional uncertainties

Recall that in this paper the probability of failure is calculated with the limit state g as

$$g_{true} = T_{allow} - T_{true}(d, r, v_0) \tag{D.1}$$

Table C1
Summary of surrogates.

Surrogate	Inputs	# of points for fitting	$PRESS_{RMS}$[a] (%)	Test e_{RMS}[b] (%)
β	$(T_{allow}-T_0)$, S, e_c	40	11	7
m	$(T_{allow}-T_0)$, S	20	0.5	0.1

[a] $PRESS_{RMS}=\sqrt{(1/p)e_{XV}^T e_{XV}}$, where p is the number of points used for fitting and e_{XV} is the vector of the difference between the true value and the surrogate prediction.

[b] $e_{RMS}=\sqrt{(1/q)e_{test}^T e_{test}}$, where q is the number of test points and e_{test} is the vector of the difference between the true value and the surrogate prediction.

Table D1
Values of the uncertain variables in the limit states.

Distribution	Before redesign	After redesign case 1	After redesign case 2
T_0		300 (deterministic)	
T_{calc}		$N(550,12.4^2)$	
ΔT_{calc}		$N(250,12.4^2)$	
T_{allow}		$LN(660,16^2)$	
e_c	$N(0,0.069^2)$[a]	$N(0,0.0621^2)$[b]	$N(0,0.035^2)$[c]

[a] This is the standard deviation of the normal distribution that is equivalent to the uniform distribution of e_c between ± 0.12 (i.e., $0.12/\sqrt{3}$).

[b] In case 1, redesign causes a 10% reduction in standard deviation of e_c.

[c] In case 2, redesign causes a 50% reduction in standard deviation of e_c.

Table D2
Standard deviation of the limit states before and after redesign. Note that the nominal value of e_c is 0.

Distribution	Before redesign	After redesign case 1 (% change)	After redesign case 2 (% change)
$\sigma_{g_{previous}}$	39.9	36.4 (−9%)	22.7 (−43%)
$\sigma_{g_{current}}$	26.8	25.7 (−4%)	22.2 (−17%)

where

$$T_{true}(d,r,v_0)=T_0(1-v_0)+(1-e_{c,true})\Delta T_{calc}(d,r) \tag{D.2}$$

Given the uncertainties in v_0, ΔT_{calc}, e_c, and T_{allow}, we can calculate the variance of the limit state as

$$\sigma_{g,current}^2=T_0^2\sigma_{v_0}^2+\sigma_{\Delta T_{calc}}^2+\Delta T_{calc}^2\sigma_{e_c}^2+\sigma_{\Delta T_{calc}}^2 e_c^2+\sigma_{e_c}^2\sigma_{\Delta T_{calc}}^2+\sigma_{T_{allow}}^2 \tag{D.3}$$

We use the subscript "current" to denote this as the limit state that is used in the current paper.

In previous work [9], the limit state was formulated as

$$g_{previous}=T_{allow}^{det}-T_{calc}(d,r)(1-e_c) \tag{D.4}$$

for which the variance is

$$\sigma_{g_{previous}}=\sigma_{T_{calc}}^2+T_{calc}^2\sigma_{e_c}^2+\sigma_{T_{calc}}^2 e_c^2+\sigma_{e_c}^2\sigma_{T_{calc}}^2 \tag{D.5}$$

In the current work, we included the additional uncertainties in the initial temperature, calculated change and temperature, and allowable temperature to form a more realistic problem.

Let us consider two cases where redesign the combination of the test and redesign reduces the standard deviation of e_c for the design listed in Table D1. The values of the uncertain variables are given in Table A1, for which the variables involved in the calculation of T_{calc} and ΔT_{calc} result in a standard deviation of 12.4 K in these values.

Using Eqs. (D.3) and (D.1), we calculate the standard deviation of the limit state g as shown in Table D2.

It was observed that the additional uncertainties, particularly the uncertainty in T_{allow}, reduced the effect of the test and redesign's reduction of σ_{e_c} on the reduction of the standard deviation of the limit state. The reductions were more than two times larger using the previous formulation, which accounts for the differences in mean and 95th percentile of the probability of failure we observed in the current work and the work in the previous paper.

References

[1] Fujimoto Y, Kim S, Hamada K. Inspection planning of fatigue deteriorating structures using genetic algorithm. J Soc Naval Archit Jpn 1997;182:729–39.
[2] Toyoda-Makino M. Cost-based optimal history dependent strategy for random fatigue cracks growth. Probab Eng Mech 1999;14(4):339–47.
[3] Garbatov Y, Soares CG. Cost and reliability based strategies for fatigue maintenance planning of floating structures. Reliab Eng Syst Saf 2001;73(3):293–301.
[4] Kale A, Haftka RT, Sankar BV. Efficient reliability-based design and inspection of panels against fatigue. J Aircr 2008;45(1):86–96.
[5] Acar E, Haftka RT, Kim NH. Effects of structural tests on aircraft safety. AIAA J 2010;48(10).
[6] Golden P, Millwater H, Dubinsky C, Singh G. Experimental resource allocation for statistical simulation of fretting fatigue problem (preprint) (Technical Report). DTIC Document; 2012.
[7] Sankararaman S, McLemore K, Liang C, Bradford SC, Peterson L. Test resource allocation for uncertainty quantification of multi-level and coupled systems. In: 52nd AIAA/ASME/ASCE/AHS/ASC structures, structural dynamics, and materials conference. Denver, CO; 2011.
[8] Venter G, Scotti SJ. Accounting for proof test data in a reliability-based design optimization framework. AIAA J 2012;50(10):2159–67.
[9] Villanueva D, Haftka RT, Sankar BV. Including the effect of a future test and redesign in reliability calculations. AIAA J 2011;49(12):2760–9, http://dx.doi.org/10.2514/1.55993.
[10] Matsumura T, Haftka RT, Sankar BV. Reliability estimation including redesign following future test for an integrated thermal protection system. In: 9th world congress on structural and multidisciplinary optimization. Shizuoka, Japan; 2011.
[11] Birge J, Louveaux F. Introduction to stochastic programming. Springer Verlag; 1997.
[12] Liu M, Sahinidis N. Optimization in process planning under uncertainty. Ind Eng Chem Res 1996;35(11):4154–65.
[13] Gupta A, Maranas C. A two-stage modeling and solution framework for multisite midterm planning under demand uncertainty. Ind Eng Chem Res 2000;39(10):3799–813.
[14] Möller N, Hansson SO. Principles of engineering safety: risk and uncertainty reduction. Reliab Eng Syst Saf 2008;93(6):798–805, http://dx.doi.org/10.1016/j.ress.2007.03.031.
[15] Aktas E, Moses F, Ghosn M. Cost and safety optimization of structural design specifications; 2001. p. 73.
[16] Beck AT, Gomes WJS, Bazan FAV. On the robustness of structural risk optimization with respect to epistemic uncertainties. Int J Uncertain Quantif 2012;2(1):1–19, http://dx.doi.org/10.1615//Int.J.UncertaintyQuantification.2011003415.
[17] Oberkampf WL, Deland SM, Rutherford BM, Diegert KV, Alvin KF. Error and uncertainty in modeling and simulation. Reliab Eng Syst Saf 2002;75:333–57.
[18] Durga Rao K, Kushwaha H, Verma A, Srividya A. Quantification of epistemic and aleatory uncertainties in level-1 probabilistic safety assessment studies. Reliab Eng Syst Saf 2007;92(7):947–56.
[19] Smarslok BP, Haftka RT, Carraro L, Ginsbourger D. Improving accuracy of failure probability estimates with separable Monte Carlo. Int J Reliab Saf 2010;4:393–414.
[20] Villanueva D, Sharma A, Haftka RT, Sankar BV. Risk allocation by optimization of an integrated thermal protection system. In: 8th world congress for structural and multidisciplinary optimization. Lisbon, Portugal; 2009.
[21] Guide to verifying safety-critical structures for reusable launch and reentry vehicles, version 1 (Technical Report). Washington, DC, USA: Federal Aviation Administration; November 2005.
[22] Rockafellar RT, Royset JO. On buffered failure probability in design and optimization of structures. Reliab Eng Syst Saf 2010;95(5):499–510.
[23] Bapanapalli SK. Design of an integrated thermal protection system for future space vehicles [Ph.D. thesis]. University of Florida; 2007.